Changes in the electronic structure and spin dynamics across the metal-insulator transition in La_{1−x}Sr_{x}CoO_{3}

R. X. Smith, M. J. R. Hoch, W. G. Moulton, P. L. Kuhns, A. P. Reyes, G. S. Boebinger, H. Zheng, and J. F. Mitchell

Phys. Rev. B **93**, 024204 — Published 25 January 2016

DOI: 10.1103/PhysRevB.93.024204

Changes in the electronic structure and spin dynamics across the metal-insulator transition in $La_{1-x}Sr_xCoO_3$

R.X. Smith,* M.J.R. Hoch, W.G. Moulton,† P.L. Kuhns, A.P. Reyes, and G.S. Boebinger
National High Magnetic Field Laboratory
Florida State University
Tallahassee, Florida 32310, USA

H. Zheng and J.F. Mitchell
Materials Science Division
Argonne National Laboratory
Argonne, Illinois 60439, USA
(Dated: December 28, 2015)

The magnetoelectronic properties of $La_{1-x}Sr_xCoO_3$, which include giant magnetoresistance, are strongly dependent on the level of hole doping. The system evolves, with increasing x, from a spin glass insulator to a metallic ferromagnet with a metal-insulator (MI) transition at $x_C \sim 0.18$. Nanoscale phase separation occurs in the insulating phase and persists, to some extent, into the just-metallic phase. The present experiments at 4.2 K have used ^{139}La NMR to investigate the transition from hopping dynamics for $x < x_C$ to Korringa-like ferromagnetic metal behavior for $x > x_C$. A marked decrease in the spin-lattice relaxation rate is found in the vicinity of x_C as the MI transition is crossed. This behavior is accounted for in terms of the evolution of the electronic structure and dynamics with cluster size.

I. INTRODUCTION

The magneto-electronic properties of the cobaltite $La_{1-x}Sr_xCoO_3$ (LSCO), which exhibit interesting emergent characteristics with increase in hole doping, have been summarized in a number of increasingly detailed phase diagrams[1–4]. The system evolves from an insulating spin glass (SG) phase at low doping ($x < 0.10$) to a ferromagnetic (FM) ordered metallic phase at high doping ($x > 0.25$). A percolation mediated insulator-metal (MI) transition occurs at $x_C \sim 0.18$. The interesting and unusual transport phenomena that are found in LSCO, including giant magnetoresistance (MR) effects, are linked to nano-scale magneto-electronic phase separation that occurs for a range of x values[3,5–12]. For $x < x_C$ the material shows large field-cooled low temperature magnetizations indicative of strong ferromagnetic correlations[3]. SG behavior is observed at low temperatures in ac susceptibility and magnetic aging experiments[11].

The Zener double exchange (DE) mechanism[13,14], which is used to account for the electronic properties of the hole-doped manganites, has been widely adopted in discussing the properties of LSCO. In contrast to the manganites, the similarity in the crystal field splitting and the Hund's rule exchange energy in LSCO leads to close competition of different spin configurations involving the occupations of the t_{2g} and e_g states[3]. The spin states for an octahedrally coordinated Co^{3+} ion are low spin (LS), $t_{2g}^6 e_g^0$ (S = 0), intermediate spin (IS) $t_{2g}^5 e_g^1$ (S = 1) and high spin (HS) $t_{2g}^4 e_g^2$ (S = 2). Because of the small energy differences between the various spin states the nature of the DE interaction between Co^{3+} and Co^{4+} ions in LSCO has been the subject of some debate.

The large MR and glassy behavior of LSCO have been accounted for using a magnetic cluster model involving short-range ordered FM regions situated in a glassy matrix[3,11,15]. The presence of short-range ordered FM regions is supported by neutron scattering on single crystals which show a finite FM correlation length for $x < x_C$ and a dramatic increase as $x \to x_C$[16]. Neutron scattering experiments suggest that an incommensurate magnetic phase coexists with FM at low temperatures for $0 < x < 0.30$[8]. Evidence for dynamic Jahn-Teller (JT) distortions in the metallic phase has been obtained in the neutron scattering experiments[16]. Small changes in rhombohedral distortion of the lattice with increasing x have been observed in neutron diffraction experiments[15].

As the MI transition is approached and crossed FM clusters merge to produce extended metallic regions. The magnetoresistance at 10 K decreases markedly as x increases from 0.1 to 0.2 corresponding to the evolution of the cluster morphology from separated clusters to the FM metallic state[9]. However, some phase separation persists above x_C with FM regions coexisting with a SG or cluster glass matrix in the range $0.04 < x < 0.22$[9,17]. In the FM metallic phase, $x > 0.22$, heat capacity results have shown a narrow conduction bandwidth and a carrier mass comparable to that in heavy fermion systems[17]. An analysis of the critical behavior of the magnetization in the vicinity of the Curie point for three selected single crystal LSCO samples with $x > x_C$ shows that the critical exponent, κ, values for $x = 0.25$ and 0.33 are close to the 3D Heisenberg model predictions for a FM while κ for the $x = 0.21$ sample is larger and close to the mean field value[18]. This finding points to the inhomogeneous ground state nature of the $x = 0.21$ sample in contrast to the homogeneous FM character of the samples with higher x values[18].

Changes in the electronic properties of bulk LSCO, as the system transforms, with increasing x, from an insula-

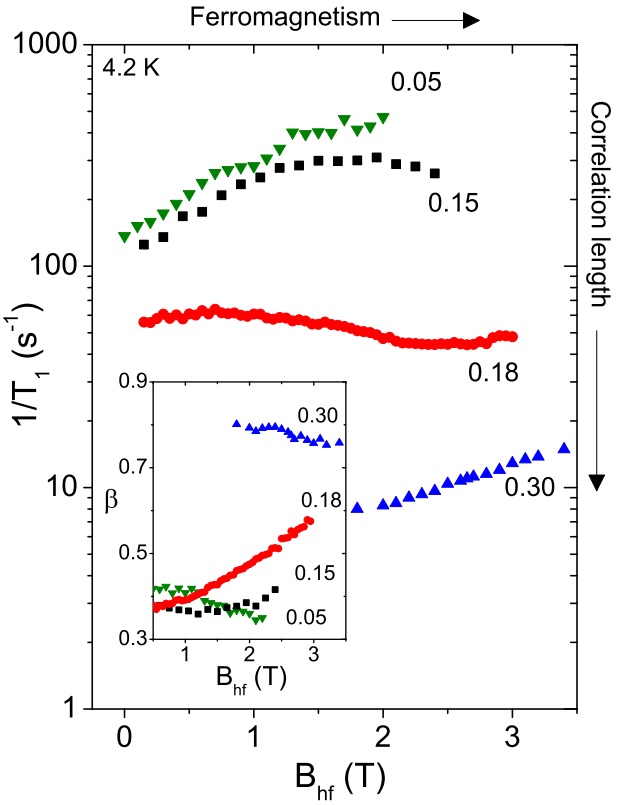

FIG. 1. (color online). Semi-log plot of the ^{139}La relaxation rates, $1/T_1$, at 4.2 K for crushed $La_{1-x}Sr_xCoO_3$ single crystals ($x = 0.05$, 0.15, 0.18 and 0.30) as a function of the ^{139}La hyperfine field B_{hf}. For $x = 0.05$, 0.15 and 0.30 there is an increase in $1/T_1$ with B_{hf}, while for $x = x_C = 0.18$ $1/T_1$ remains roughly constant. These trends are discussed in the text. The $1/T_1$ values at $B_{hf} = 2$ T show a marked decrease with x as presented in detail in Fig. 2. The text with arrows (top and right hand axes) provides a guide to the property changes with increasing x and decreasing $1/T_1$. The inset shows a plot of the stretched exponential exponent β (defined in the text) vs. B_{hf} . The increase in β with x, and in certain regions with B_{hf}, points to a decrease in the width of the relaxation rate distribution as the material becomes metallic.

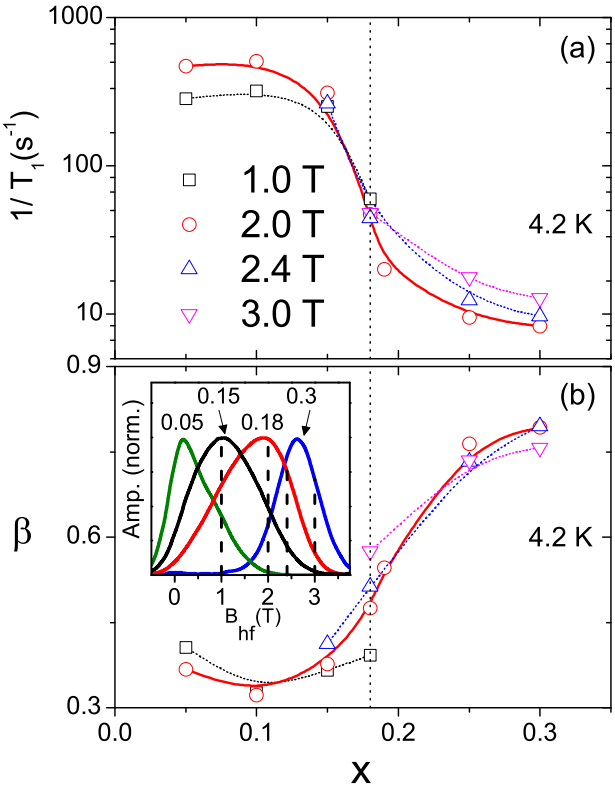

FIG. 2. (color online).(a) ^{139}La $1/T_1$ values for LSCO as a function of x at 4.2 K for selected B_{hf} values (1, 2, 2.4 and 3 T) as indicated in the Fig.2(b) inset which shows ^{139}La NMR spectra, at 4.2 K, as a function of B_{hf}. In Fig.2(a) there is a marked decrease in $1/T_1$ near the MI transition at $x_C = 0.18$ due to changes in the electronic structure as the transition is crossed. (b) Stretched exponential exponent β vs. x showing a marked increase across the MI transition. The observed change in β above x_C is consistent with an increase in homogeneity in the FM metallic phase as discussed in the text.

tor to a FM metal, have been investigated using density functional theory calculations[19–21]. For $x < 0.2$ the results support the model of mixed valence Co ions and phase separation involving metallic clusters in a hole-poor, low spin (LS) matrix. For $x > 0.2$ the calculations predict that phase separation is no longer significant and that a metallic phase emerges[21]. A recent dynamical mean-field theory combined with density functional theory (DFT + DMFT) approach indicates that coherent t_{2g} bands emerge at the Fermi level for $x > 0.2$. The analysis suggests that the DE mechanism with an e_g conduction band is not appropriate for the metallic phase of LSCO[22].

The magnetic and electronic properties of $x = 0.3$ LSCO films, measured as a function of epitaxial strain, are consistent with a narrow t_{2g}-derived conduction band[23]. The narrow t_{2g} band in LSCO contrasts with the larger bandwidth of the e_g-derived band in the doped manganites. This bandwidth difference is consistent with estimates based on NMR spin-lattice relaxation rate results for the $x = 0.3$ samples of these two oxides[24]. The recent findings for LSCO suggest that the DE interaction in LSCO involves the t_{2g} derived states of HS Co^{3+} ($t_{2g}^4 e_g^2$) and Co^{4+} ($t_{2g}^3 e_g^2$) ions[20,23].

X-ray magnetic circular dichroism (XMCD) measurements on single crystals of LSCO have revealed that hole doping induces magnetic oxygen hole states with moments that vary with x[20]. Complementary theoretical calculations show that the O moments depend on the number of Sr neighbors[20]. The hybridization of the Co 3d states with O 2p states plays an important role in establishing large transferred hyperfine fields at neighboring ^{139}La sites which can be probed using magnetic resonance techniques[6]. Using this approach information on the evolution of the spin dynamics with temperature has been obtained for a set of LSCO samples with x val-

ues in the range 0.05 - 0.3[4]. The findings have been incorporated into the phase diagram for this system[4].

The present low temperature ^{139}La NMR experiments reveal changes in the spin dynamics which accompany the MI transition. This behavior is explained using expressions which allow for changes in the electronic states of the system with x.

II. EXPERIMENTAL DETAILS AND RESULTS

The LSCO single crystal samples, which were grown in a floating zone furnace, were crushed to a mean size of 20 μm to minimize skin depth effects in the metallic material. The ^{139}La (I = 7/2, $^{139}\gamma/2\pi$ = 6.015 MHz/T) measurements were made at 4.2 K in a field-sweep superconducting magnet, with fields in the range 10 – 14 T. A pulsed NMR spectrometer, operating at 84.2 MHz, was used to record spectra from spin-echo responses as described previously[4]. In LSCO, the transferred hyperfine interactions at ^{139}La sites, produced primarily by the nearest-neighbor Co ions via surrounding octahedral O atoms, give rise to a local field B_{hf} which, to a good approximation, is directed along the applied field. Rapid exchange processes average the hyperfine field over the different spin states of the neighbor Co ions involved in the process. Variations in B_{hf} from hole-rich to hole-poor regions of the Sr doped crystals give rise to a distribution of ^{139}La spectral shifts from < 0 T to > 4 T. Broad NMR lines are found for samples over a wide range of x values[4].

Figure 1 shows the $1/T_1$ values at 4.2 K as a function of B_{hf} for four samples in a semi-log plot. Figure 2a plots $1/T_1$ as a function of x for particular B_{hf} values in the range 1 – 3 T. Sigmoidal curves are fit to the data as shown. The inset in Fig. 2b gives the 4.2 K ^{139}La spectral shapes for x = 0.30, 0.18, 0.15, and 0.05, as a function of hyperfine field shift, B_{hf}, measured from the ^{139}La resonance field in a non-magnetic environment. The observed range of B_{hf} values, and the asymmetric shapes of the ^{139}La spectra have been discussed previously using a statistical cluster model for the Sr ion distribution in the lattice[4]. Below x_C, the x = 0.05 and 0.15 results show $1/T_1$ increasing by roughly a factor of 5 as B_{hf} increases from 0.5 to 2.5 T. For x = 0.18, however, the trend across the spectrum is different with the $1/T_1$ values decreasing slightly for B_{hf} > 1 T. For $x > x_C$, where the FM correlation length diverges[16], the $1/T_1$ values are markedly lower, by more than an order of magnitude, than for $x < x_C$.

Because of the large linewidths, with full-width-half-maximum (FWHM) values of 1 to 2 T (6 – 12 MHz), the relaxation rate measurements were made using hole-burning procedures across the spectrum. The RF pulse lengths $\sim$ 2.5 μs correspond to a spectral width of 400 kHz (0.06 T) which is much less than the linewidth. The behavior of the ^{139}La spin-lattice relaxation rate with temperature for LSCO is discussed in Ref. 4 in terms of

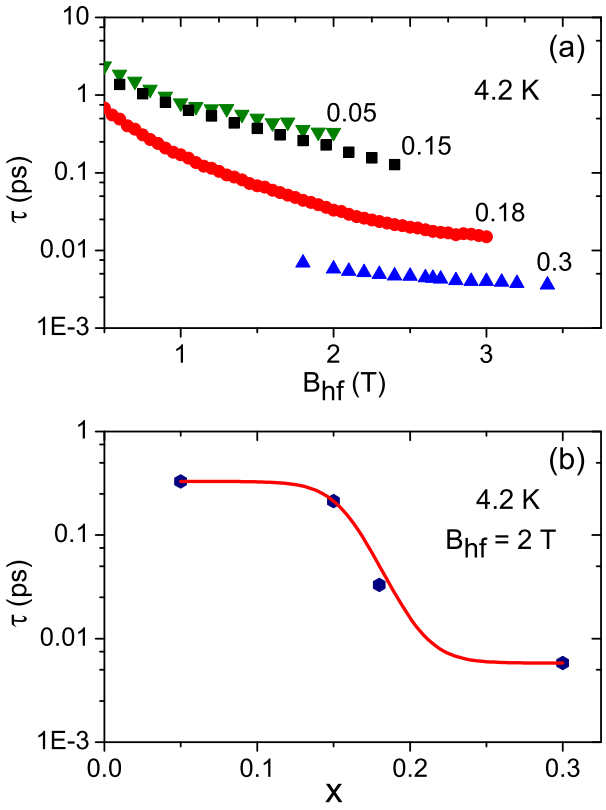

FIG. 3. (color online). (a) Correlation times, τ, for the hyperfine field fluctuations at ^{139}La sites in LSCO as a function of the average B_{hf} for x = 0.05, 0.15, 0.18 and 0.3. The values are derived from $1/T_1$ for ^{139}La at 4.2 K with use of Eq. (A4) as described in the text. The τ values for x = 0.3, are consistent with Eq. (A3), and are shown for comparison purposes with those for $x \leq x_C$. (b) Correlation times τ at B_{hf} = 2 T as a function of x. The sigmoidal curve through the points is a guide to the eye.

thermally activated processes. These processes are not expected to play a significant role in low temperature nuclear relaxation in FM clusters.

The nuclear magnetization recovery curves, used to measure $1/T_1$, exhibit stretched exponential behavior at low temperatures given by the form $M/M_0 = 1-e^{-(t/T_1)^\beta}$ where M_0 is the equilibrium nuclear magnetization at a given temperature with the exponent $\beta \leq 1$ which implies a distribution of T_1 values. Low β values corresponds to broad T_1 distributions and provide a signature of magnetic inhomogeneity in LSCO.[25]. For $\beta \sim 0.7$ the distribution has a FWHM $\Delta T_1 \sim T_1$ and the distribution increases in width for smaller β values[16].

The inset in Fig. 1 gives β as a function of B_{hf} for the four x values shown. For $x \leq 0.18$ we find that $\beta < 0.5$ over the range $0 < B_{hf} < 2$ T. Gradual changes in β occur with increase in B_{hf}. For x = 0.3 we have $B_{hf} > 0.75$ and, within experimental uncertainty, the value remains roughly constant for $2 < B_{hf} < 3.5$ T. Inspection of the $1/T_1$ vs. B_{hf} and β vs. B_{hf} plots provides a clear indica-

tion of the very different natures of the FM regions for x above and below x_C. Large B_{hf} values occur both in local clusters ($x < x_C$) and in extended metallic regions ($x > x_C$) which have quite different NMR relaxation properties. Figure 2b shows β vs. x for four selected B_{hf} values, as indicated in the inset in Fig. 2a, together with sigmoidal fit curves. In contrast to the marked decrease in $1/T_1$ with x in Fig. 2a, β increases from 0.35 to 0.8 as x passes through x_C. The increase is consistent with a change from a broad distribution of T_1 values in the inhomogeneous insulating phase to a narrower distribution in the more homogeneous metallic phase.

The spin-echo decay curves from which the spin-spin relaxation rate, $1/T_2$, can be obtained (not shown) are well fit with single exponentials for $x < x_C$ and with Gaussian functions for $x > x_C$. At 4.2 K the $1/T_2$ values exhibit little change across the spectrum, for any x value, but do show a small decrease for $x > x_C$. In Section III we examine the behavior of $1/T_1$ as a function of x and B_{hf}.

III. DISCUSSION

The 4.2 K relaxation rates, plotted vs. B_{hf} in Fig. 1, and vs. x, for selected B_{hf} values in the range 1 - 3 T, in Fig. 2a, exhibit a marked dependence on x as the MI transition is approached and crossed. The $1/T_1$ values at 2 T in Fig. 2a show two distinct quasi-plateau regions; firstly for $0.05 < x \leq 0.1$, and secondly for $x \geq 0.25$, with a large step-like decrease in $1/T_1$ near x_C. Similar low x plateau behavior is found for the relaxation rates at B_{hf} = 1 T. The $1/T_1$ values at 1 T and 2 T converge for $x \rightarrow x_C$ as is evident in Fig. 2a. It is clear that the spin-lattice relaxation mechanism, at constant B_{hf}, evolves dramatically with x across x_C.

In comparing nuclear relaxation rates at particular hyperfine fields in samples with different x values it is important to note that for $x < x_C$ large B_{hf} values can occur in regions with a broad distribution of sizes. These regions include small clusters, with dimensions of the order of several lattice distances, in which there are large Sr concentrations as detected by neutron scattering experiments[16]. The neutron scattering measurements show diverging FM correlation lengths for $x \rightarrow x_C$ as clusters grow and coalesce[16]. As mentioned in section I, recent x-ray absorption spectroscopy and x-ray magnetic circular dichroism experiments on LSCO have shown that a small but significant part of the local spin moment due to hole doping is located on the O atoms. The moments at a particular O site are sensitive to the number of adjacent Sr ions[20]. This finding helps in understanding the broad distribution of transferred hyperfine fields at ^{139}La sites.

It is interesting to note that the coercive field at 5 K decreases by roughly an order of magnitude as x approaches and passes through x_C[26]. The change is attributed to the transition from magnetization rotation in separated clusters to domain wall motion in the FM metallic phase[26]. The behavior of the coercive field with increasing x is very similar in form to that of the NMR relaxation rate in Fig. 2a which suggests that both quantities are linked to the emergent cluster properties. Neutron scattering has shown that for $x = 0.15$ at low T the correlation length for FM clusters is $\sim 1.5 - 2.5$ nm[7]. The electronic structures in these small regions differ from those for $x > x_C$ in which metallic regions are present with a Fermi surface and a quasi-continuum of electron states. The electron dynamics correspondingly evolve with increase in x. The changes in $1/T_1$ with x reflect the changes in the electronic structure. We note that a hopping mechanism has been invoked to explain the relaxation of ^{139}La in the manganite $La_{1-x}Na_xMnO_3$[27].

The appendix gives expressions for ^{139}La spin-lattice relaxation rates, firstly for $x > x_C$ in Eq. (A3), and, secondly for $x < x_C$ in Eq. (A4). For $x > x_C$ the approach is based on an anisotropic hyperfine model introduced previously for nuclear relaxation (^{59}Co or ^{55}Mn) in metallic cobaltites and manganites[24]. Equation (A3) is shown to be similar in form to the Moriya relation for magnetic metals[28] given in Eq. (A1).

Using the Moriya expression in Eq. (A1) the 4.2 K ^{59}Co relaxation rates for LSCO with $x = 0.3$ have previously been analyzed with the density of states $\rho(E_F) = 22.8$ eV^{-1} based on electronic specific heat measurements[29]. As an approximation it is assumed that $\rho_\uparrow^2 \approx \rho^2$ for this FM metal[24]. The experimental value for the ^{59}Co $1/T_1T$ value is $\sim$300 (sK)$^{-1}$ and this is in agreement with the estimate obtained using the above value for $\rho(E_F)$ with Eq. (A1) and taking $F(\Gamma)$=1[24]. The agreement between theory and experiment for ^{59}Co relaxation confirms the FM metal nature of the $x = 0.3$ LSCO sample from an NMR perspective. Equation (A1) can be adapted to the *transferred* hyperfine field induced ^{139}La relaxation in metallic $La_{0.7}Sr_{0.3}CoO_3$ by using the density of states for this system, as given above, and the ratio of the measured $1/T_1T$ values in order to estimate the effective transferred hyperfine field at ^{139}La sites. The experimental value from Fig. 2a of $1/T_1T \approx 2.4$ (sK)$^{-1}$ gives $\left\langle B_1^{La} \right\rangle_F \sim 1.4$ T.

Qualitatively, the behavior of $1/T_1$ as a function of x, at *constant* B_{hf}, as shown in Fig. 2a, is described as a transition from exchange mediated relaxation in finite clusters for $x < x_C$, to itinerant electron scattering in extended metallic regions for $x > x_C$. In this picture, the $x < x_C$ plateau regions in $1/T_1$ in Fig. 2a correspond to the product $\left\langle \Delta B_{hf} \right\rangle_{Ins}^2 \tau$ remaining approximately constant as x increases. As x approaches and passes through x_C the electronic structure evolves with the magnetic clusters merging into long-range ordered structures with a Fermi surface. When the itinerant electron conduction band is established the ^{139}La relaxation rate, at particular B_{hf} values, tends towards fully developed FM metal behavior giving the plateau at high x in Fig. 2a.

On the insulating side of the MI transition where FM nanoclusters of varying sizes are important the analysis of

the ^{139}La relaxation rate results can be carried out only by making a number of assumptions about the parameters involved in Eq. (A4). We assume that the amplitude of the fluctuating hyperfine field is proportional to the static average field and take $\left\langle B_1^{La} \right\rangle = f\mathrm{B}_{hf}$ with the factor $f < 1$. Based on the estimate of $\left\langle B_1^{La} \right\rangle$ obtained for the metallic $x = 0.3$ sample using Eq. (A1), as given above, we choose $f \sim 0.5$. This fairly crude assumption ignores dopant-dependent local structural distortions, including Jahn-Teller distortions, which may alter the fluctuating transferred hyperfine interaction at ^{139}La sites. The approach used provides a semiquantitative analysis of the experimental results in the insulating phase.

From the $1/T_1$ data in Fig. 1, making use of Eq. (A4) for $x < x_{\mathrm{C}}$, with $\left\langle B_1^{La} \right\rangle = \frac{1}{2}\mathrm{B}_{hf}$ we obtain the correlation time τ as a function of x for $\mathrm{B}_{hf} = 2$ T as shown in Fig. 3b. The data are fit with a sigmoidal curve. For comparison purposes, and based on the discussion given above, τ values are also shown for the $x = 0.3$ sample using Eq. (A4). The estimated values should be viewed with caution, particularly in the vicinity of the MI transition and for $x > x_{\mathrm{C}}$. Nevertheless, the analysis provides insight into the evolution of the electronic properties with increased hole doping. Figure 3b suggests that τ decreases by close to two orders of magnitude as x increases from 0.05 to 0.3.

Figure 3b shows that for $x = 0.05$ and $x = 0.15$ the τ values are very similar and decrease from ~ 2 ps to ~ 0.2 ps as B_{hf} increases from 0.5 to 2.0 T. The gradual decrease in τ with B_{hf} on the insulating side of the MI transition is determined by the relatively weak dependence of $1/T_1$ on B_{hf}. For the $x = 0.18$ sample the τ values are significantly shorter than for $x < x_{\mathrm{C}}$. The marked decrease in τ at $x = x_{\mathrm{C}}$ is, however, qualitatively consistent with expectations as the metallic phase is entered and the Fermi surface is established in extended regions.

For $x < x_{\mathrm{C}}$ the gradual almost linear increase in $1/T_1$ with hyperfine field in the range B_{hf} as shown in Fig. 1, should, from Eq. (A4), have the form $1/T_1 \propto (B_{hf})^2 \tau$ as given above. We note that for x values 0.05 and 0.15 the calculated slopes from Fig. 1 ($\mathrm{B}_{hf} < 2$ T) are significantly less than 2 and, in terms of the proposed relaxation model, it follows that across the spectrum the effect of an increase in ΔB_{hf} on $1/T_1$ is largely offset by a decrease in τ. This conclusion is supported by the observation that for $\mathrm{B}_{hf} > 1.5$ T the $1/T_1$ values for $x = 0.15$ pass through a maximum and then decrease. The featureless behavior of $1/T_1$ as a function of B_{hf} for $x = 0.18$ in Fig. 1 is consistent with mixed phase character at the MI transition.

It is possible that for $x < x_{\mathrm{C}}$ both intra-cluster and inter-cluster hopping processes, which are important for electrical transport, contribute to the ^{139}La relaxation rate. However, examination of Fig. 1 shows that $1/T_1$ decreases as x is increased from 0.05 to 0.15. This small change in the relaxation rate with x points away from an inter-cluster hopping mechanism being significant in nuclear relaxation at 4.2 K and indicates that intra-cluster exchange plays the major role.

In summary, our low temperature ^{139}La relaxation rate measurements on LSCO have probed the evolution of changes in the electronic structure with x across the MI transition at x_{C}. In the insulating phase the correlation times for hyperfine field fluctuations at ^{139}La sites are found to depend on x. The results are consistent with the development of magnetic clusters with increasing x which give rise to a percolation transition at x_{C}. Estimates are made of the exchange correlation times in the less metallic and more metallic sample regions. For $x > x_{\mathrm{C}}$ a conduction band characterized by a density of states at the Fermi level is established as the clusters coalesce and form extended metallic regions. A dramatic change in the 4.2 K ^{139}La spin-lattice relaxation rate occurs at the MI transition as a result of changes in the electronic structure and associated changes in the electron spin dynamics.

IV. CONCLUSION

The present ^{139}La NMR measurements made on LSCO as a function of hole-doping is at low temperatures reveal that the spin-lattice relaxation rate undergoes a large decrease, by close to two orders of magnitude, in the vicinity of the MI transition. This behavior is linked to the change in the electronic structure from localized cluster states in the insulating phase to itinerant metallic states in the conduction band for $x > x_{\mathrm{C}}$. The results are analyzed using an approach which allows for changes in the electronic structure, and hence in the electron spin dynamics, as x is increased through x_{C}.

ACKNOWLEDGMENTS

The work at the National High Magnetic Field Laboratory was supported by National Science Foundation Cooperative Agreement No. DMR-1157490 and the State of Florida. We thank Chris Leighton of the University of Minnesota for his helpful comments and advice. Work in the Materials Science Division of Argonne National Laboratory (crystal growth, sample characterization) is supported the U.S. Department of Energy, Office of Science, Basic Energy Sciences, Materials Science and Engineering Division.

Appendix A: NMR SPIN-LATTICE RELAXATION EXPRESSIONS FOR LSCO

The classic Moriya relaxation rate expression[28] for the magnetic ions in a ferromagnetic metal, such as cobalt, in which the orbital processes have been shown to be of dominant importance can be written as[24]

$$\frac{1}{T_1} = C\Big\langle B_{hf}\Big\rangle_F^2 \Big(\rho_\uparrow^2 + \rho_\downarrow^2\Big) F(\Gamma) T, \qquad \text{(A1)}$$

where $C = (16\pi/5)\gamma_I^2 \hbar k_B$ and $\langle B_{hf}\rangle_F = \mu/\langle r_A^3\rangle_F$ is the d-electron orbital field with $1/\langle r_A^3\rangle_F$ the inverse radius cubed averaged over the Fermi surface of the d band, γ_I is the nuclear gyromagnetic ratio and $\rho_\uparrow$ and $\rho_\downarrow$ are the densities of states at the Fermi energy, E_F, for spin up and spin down electrons, respectively. The function $F(\Gamma)$ gives a measure of the t_{2g} orbital admixture in the wave function at E_F, with a maximum value of unity[28,30]. Equation (A1) has been used[24] to analyze the ^{59}Co relaxation rates for $La_{0.7}Sr_{0.3}CoO_3$ using the density of states from electronic specific heat measurements as discussed in Section III.

For hole-doped noncubic perovskites, such as the cobaltites, with $x > x_c$, a somewhat different approach has been proposed to describe nuclear spin-lattice relaxation of the transition metal ion nucleus. The approach involves fluctuations in the local hyperfine field characterized by a correlation time[24]. The model allows for *a*nisotropy in the hyperfine interaction. We adapt the model to the case of relaxation due to time-dependent *t*ransferred hyperfine fields at ^{139}La sites in LSCO. The Hamiltonian has the form $H = I \cdot A \cdot S$ where I is the ^{139}La nuclear spin operator and S the Co ion electron spin operator with A the hyperfine tensor. We assume that S and I are quantized along different directions z and z' oriented at an angle α to one another. The principal values of A are denoted $A_i (i = 1, 2 \text{ and } 3)$. As shown in Ref. 24, with y and y' chosen to coincide, the Hamiltonian can be written as

$$H = A_1 I_{x'} S_z \sin\alpha + \frac{1}{2} A_3 I_{z'} S_z \cos\alpha + ... \qquad \text{(A2)}$$

The dots represent terms containing the S spin raising and lowering operators which are omitted since S spin-flip processes are unimportant at low temperatures in this ferromagnetic system. Note that $I_{x'}$ can be expressed in terms of the I spin raising and lowering operators. The first term in Eq. (A2) is responsible for spin-lattice relaxation while the second term plays a major role in spin-spin relaxation. It is convenient to put $\gamma_I\ B_1 = A_1\ S_z\ \sin\alpha$ in Eq. (A2) and to use this form in obtaining the time correlation function $G_1(\tau) = \langle B_1(\tau) B_1(0)\rangle$ of the fluctuating transverse hyperfine field. The spectral density is obtained by taking the Fourier transform of the correlation function assuming the exponential decay form with correlation time τ. The hyperfine field fluctuations occur in the short correlation time limit with $\omega_I \tau << 1$.

In order to proceed we generalize the approach and distinguish between two limiting cases. The first corresponds to a metallic system with a Fermi surface and Fermi energy E_F. Only states with energies close to E_F participate in relaxation and we have

$$\frac{1}{T_1} = \gamma_I^2 B_1^2 (\frac{T}{T_F}) \tau_F. \qquad \text{(A3)}$$

In this metallic limit we take the time $\tau_F \approx \hbar/E_F = \hbar/k_B T_F$[31] and insertion into Eq. (A3) with $\rho(E_F) \approx N/E_F$ gives an equation of the form of Eq. (A1) differing only in a numerical factor. On the insulator side of the MI transition the density of states in nanoclusters ($\propto N$) is low with states separated by energies comparable to or possibly greater than $k_B T$. In this limit we take

$$\frac{1}{T_1} = \gamma_I^2 B_1^2 \tau, \qquad \text{(A4)}$$

which is of the form of the expression for nuclear relaxation due to a fluctuating local field obtained using Redfield theory[32]. The transition from Eq. (A3) to Eq. (A4) occurs across the MI transition as the carrier (hole) dynamics change from itinerant scattering in the metallic phase, characterized by the time τ_F, to local exchange processes, with correlation time τ, in the FM nanoclusters. We are likely to have a distribution of correlation times, corresponding to a distribution of α due to factors such as Jahn-Teller distortions in these complex systems. It follows that the nuclear magnetization recovery curves are likely to display stretched exponential behavior as observed in the experiments. Equations (A3) and (A4) are used in the discussion of the LSCO relaxation rates given in Section III.

* New address: Laboratory of FMRI Technology (LOFT), Department of Neurology, Ahmanson-Lovelace Brain Mapping Center, University of California, Los Angeles, California

† Deceased

[1] M. A. Señaris-Rodriguez and J. B. Goodenough, J. Solid State Chem. **118**, 323 (1995).

[2] M. Itoh, L. Natori, S. Kubota, and K. Motoya, J. Phys. Soc. Japan **63**, 1486 (1994).

[3] J. Wu and C. Leighton, Phys. Rev. B **67**, 174408 (2003).

[4] R. X. Smith, M. J. R. Hoch, W. G. Moulton, P. L. Kuhns, A. P. Reyes, G. S. Boebinger, H. Zheng, and J. F. Mitchell, Phys. Rev. B **86**, 054428 (2012).

[5] P. L. Kuhns, M. J. R. Hoch, W. G. Moulton, A. P. Reyes, J. Wu, and C. Leighton, Phys. Rev. Lett. **91**, 127202 (2003).

[6] M. J. R. Hoch, P. L. Kuhns, W. G. Moulton, A. P. Reyes, J. Lu, J. Wu, and C. Leighton, Phys. Rev. B **70**, 174443 (2004).

[7] J. Wu, J. W. Lynn, C. J. Glinka, J. Burley, H. Zheng, J. F.

Mitchell, and C. Leighton, Phys. Rev. Lett. **94**, 037201 (2005).
[8] D. Phelan, D. Louca, K. Kamazawa, S.-H. Lee, S. Rosenkranz, M. F. Hundley, J. F. Mitchell, Y. Motome, S. N. Ancona, and Y. Moritomo, Phys. Rev. Lett. **97**, 235501 (2006).
[9] C. He, S. El-Khabib, J. Wu, J. W. Lynn, H. Zheng, and J. F. Mitchell, Europhys. Lett. **87**, 27006 (2009).
[10] C. He, S. El-Khabib, S.Eisenberg, M. Manno, J. Lynn, H. Zheng, and J. F. Mitchell, Appl. Phys. Lett. **95**, 222511 (2009).
[11] Y. K. Tang, Y. Sun, and Z.-H. Cheng, Phys. Rev. B **73**, 012409 (2006).
[12] D. Phelan, D. Louca, S. N. Ancona, S. Rosenkranz, H. Zheng, and J. F. Mitchell, Phys. Rev. B **79**, 094420 (2009).
[13] C. Zener, Phys. Rev. **82**, 403 (1951).
[14] P. Anderson and H. Hasegawa, Phys. Rev. **100**, 675 (1955).
[15] R. Caciuffo, D. Rinaldi, G. Barucca, J. Mira, J. Rivas, M. A. Señaris-Rodriguez, P.G.Radaelli, D. Fiorani, and J. B. Goodenough, Phys. Rev. B **59**, 1068 (1999).
[16] D. Phelan, D. Louca, S. Rosenkranz, S.-H. Lee, Y. Qiu, P. J. Chupas, R. Osborn, H. Zheng, J. F. Mitchell, J. R. D. Copley, J. L. Sarrao, and Y. Moritomo, Phys. Rev. Lett. **96**, 027201 (2006).
[17] C. He, S. Eisenberg, C. Jan, H. Zheng, J. F. Mitchell, and C. Leighton, Phys. Rev. B **80**, 214411 (2009).
[18] N. Khan, P. Mandal, K. Mydeen, and D. Prabhakaran, Phys. Rev. B **85**, 214419 (2012).
[19] P. Ravindran, H. Fjellvøag, A. Kjekshus, P. Blaha, K. Schwarz, and J. Luitz, J. Appl. Phys. **91**, 291 (2002).
[20] S. Medling, Y. Lee, H. Zheng, J. F. Mitchell, J. W. Freeland, B. N. Harmon, and F. Bridges, Phys. Rev. Lett. **109**, 157204 (2012).
[21] K. Knižek, Z. Jirák, J. Hejtmánek, and P. Novak, J. Magn. And Magn. Mater. **322**, 1221 (2010).
[22] P. Augustinský, V. Křápek, and J. Kuneš, Phys. Rev. Lett. **110**, 267204 (2013).
[23] D. Fuchs, M. Merz, P. Nagel, R. Schneider, S. Schuppler, and H. von Löhneysen, Phys. Rev. Lett. **111**, 257203 (2013).
[24] M. J. R. Hoch, P. L. Kuhns, W. G. Moulton, A. P. Reyes, M. A. Torija, J. F. Mitchell, and C. Leighton, Phys. Rev. B **75**, 104421 (2007).
[25] D. C. Johnston, Phys. Rev. B **74**, 184430 (2006).
[26] H. M. Aarbogh, J. Wu, L. Wang, H. Zheng, J. F. Mitchell, and C. Leighton, Phys. Rev. B **74**, 134408 (2006).
[27] M. M. Savosta, V. A. Borodin, and P. Novak, Phys. Rev. B **59**, 8778 (1999).
[28] T. Moriya, J. Phys. Soc. Japan **19**, 681 (1964).
[29] M. Paraskevopoulos, U. Hemberger, A. Krimmel, , and A. Lodl, Phys. Rev. B **63**, 224416 (2001).
[30] Y. Obata, J. Phys. Soc. Japan **18**, 1020 (1963).
[31] A. Abragam, *The Principles of Nuclear Magnetism* (Oxford University Press, Oxford, 1961).
[32] C. P. Slichter, *Principles of Magnetic resonance, 3rd ed* (Springer-Verlag, Heidelberg, 1996).